OS16-03-3

The 12th International Symposium on Fluid Control, Measurement and Visualization
November18-23, 2013, Nara, Japan
FLUCOME2013

Numerical Simulation of Mechanical Energy Transfer between Fluid and a Circular Cylinder Forced to Follow an Elliptical Path

L. Baranyi
Department of Fluid and Heat Engineering, University of Miskolc, Miskolc, Hungary
E-mail: arambl@uni-miskolc.hu

ABSTRACT

Low-Reynolds number two-dimensional flow around a circular cylinder forced to follow an elliptical path and placed in a uniform stream is investigated numerically using a thoroughly tested finite difference code. Mechanical energy transfer E and time-mean of lift and drag are investigated within the lock-in domain against the transverse oscillation amplitude for Reynolds numbers Re=150 and 200 and frequency ratios 0.8, 0.9 and 1.0 at six different in-line to transverse oscillation amplitude ratio values. The main objective of the paper is to investigate the effects of the shape of the cylinder path (amplitude ratio) and of frequency ratio on the time-mean of lift and drag coefficients and especially on the mechanical energy transfer between the fluid and cylinder. Findings show that both the frequency and amplitude ratios have important effects on the positive E values that may play important roles in the vortex-induced vibration (VIV) of elastically supported cylinders.

Keywords: *circular cylinder*, *drag*, *lift*, *mechanical energy transfer*, *Reynolds number*

1. INTRODUCTION

Flow past circular cylinders has been studied as a prototype of bluff body flows theoretically, experimentally and numerically. Some examples of these are smokestacks or silos in wind or underwater pipes in a current. When vortices are shed from the body a periodic force is generated which may result in the vibration of the structure, especially if the damping is small and the frequency of vortex shedding is near to the natural frequency of the structure. These vibrations may lead to the damage of the structure or noisy operation of heat exchangers. Due to its practical importance there is a growing interest in dealing with cylinders in motion. Many researchers have dealt with one-degree-of-freedom (1-DoF) motion, most frequently cylinder oscillation transverse to the main stream (see e.g. [1, 2, 3, 4]). This 1-DoF motion has been observed in silos, chimneys and other slender structures. The other type of 1-DoF motion is in-line with the main stream (see e.g. [5, 6]) which also occurs in reality.

In most cases, however, vibration occurs in both transverse and in-line (streamwise) directions, leading to a two-degree-of-freedom (2-DoF) motion. Relatively few studies deal with either free or forced 2-DoF motions, two types of which have been observed in practice: (a) when the frequency of cylinder oscillation in streamwise direction is double that of the transverse direction ($f_x=2f_y$), yielding a figure-8 path (see e.g. [7, 8, 9]), and (b) when the oscillation frequencies in the two directions are identical ($f_x=f_y=f$), resulting in an elliptical path (e.g. [10, 11]). To the best knowledge of the author investigations related to flow around orbiting cylinders are very limited in spite of the fact that pipes in the tube bundles of heat exchangers often follow this kind of path [12]. The free-vibration experimental study of Kheirkhah et al. [9] found that the transverse oscillation amplitude is larger than the in-line amplitude, leading to a slender elliptical path.

The main objective of this paper is to investigate the effect of several parameters (ratio of streamwise and transverse amplitudes (limited to slender cylinder paths), ratio of cylinder oscillation frequency and frequency of vortex shedding from a stationary cylinder at the same Reynolds number, transverse oscillation amplitude and Reynolds number), focussing on the positive values of mechanical energy transfer between the fluid and the cylinder.

2. COMPUTATIONAL METHOD AND SETUP

A non-inertial system fixed to the accelerating cylinder is used for the computation of the two-dimensional (2D), constant property, low-Reynolds number incompressible fluid flow around a circular cylinder placed in a uniform stream. The governing equations are the non-dimensional Navier-Stokes equations in a non-inertial system fixed to the moving cylinder, the equation of continuity and a Poisson equation for pressure.

A no-slip boundary condition is used for the velocity and a Neumann type boundary condition for the pressure is used on the cylinder surface. At the far region potential flow is assumed. Computational results show that this assumption results in some inaccuracies near the outlet boundary only, and practically it does not influence the near-wake flow and forces acting on the cylinder.

Boundary-fitted coordinates are used in order to impose the boundary conditions accurately. The physical domain, which is bounded by two concentric circles with radii R_1 and R_2, is transformed into a rectangular computational domain with equidistant spacing (see Fig. 1). This mapping ensures a fine grid scale near the cylinder and a coarse grid in the far field. The transformed governing equations and boundary conditions are solved by the finite difference method. A third-order upwind scheme is used for the convective terms; other space derivatives are approximated by fourth-order central differences. The Poisson equation for pressure is solved by the successive over-relaxation (SOR) method. The equations of motion are integrated explicitly in time and continuity is satisfied at every time step. For further details see [11]. The code developed by the author has been extensively tested against experimental and computational results and good agreement was found (see [11]). In this study the dimensionless time step is 0.0005, the computational domain is characterised by R_2/R_1=160 and the grid is 361x292.

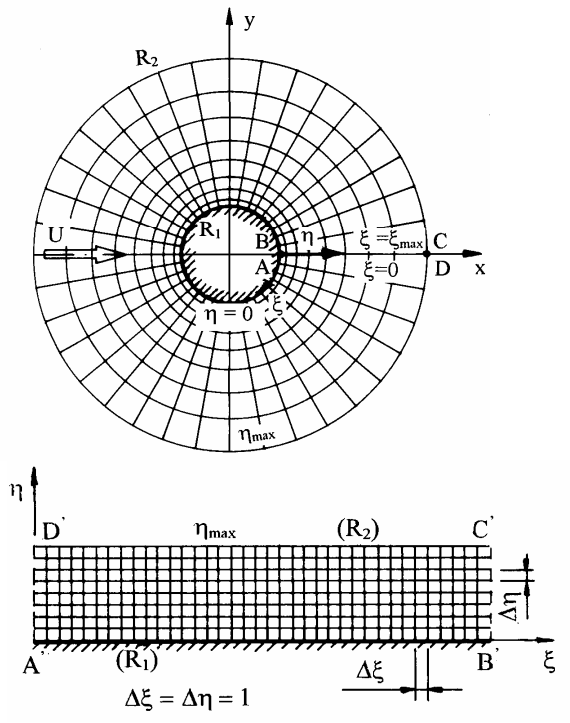

Figure 1: Physical and computational planes

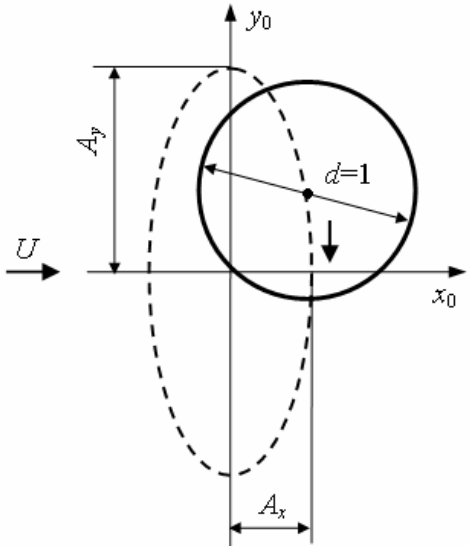

Figure 2: Layout of cylinder path

The layout of the cylinder path is shown in Fig. 2. Here U is the free stream velocity (and velocity scale), $d=2R_1$ is the cylinder diameter (and length scale), and A_x and A_y are the dimensionless amplitudes in x and y directions, respectively. Every quantity is made dimensionless by the combination of U and d. The dimensionless displacements of the forced cylinder motion x_0, y_0 in x and y directions are given by

$$x_0=A_x \cos(2\pi f t); \qquad y_0=-A_y \sin(2\pi f t), \tag{1}$$

where f is the cylinder oscillation frequency (identical in x and y directions) non-dimensionalized by U/d. Equation (1) ensures a clockwise direction of orbit. The following notations are used for the amplitude ratio ε and frequency ratio FR

$$\varepsilon=A_x/A_y, \tag{2}$$

$$\mathrm{FR}=f/\mathrm{St}_0, \tag{3}$$

where f is the dimensionless cylinder oscillation frequency in both x and y directions and St_0 is the vortex shedding frequency from a stationary cylinder at the same Reynolds number. Reynolds number is defined as $\mathrm{Re}=Ud/\nu$, where ν is the kinematic viscosity of the fluid.

Throughout this paper the lift (C_L) and drag (C_D) coefficients used do not contain the inertial forces originating from the non-inertial system fixed to the moving cylinder. These coefficients are often termed 'fixed body' coefficients (see [2]). The two sets of coefficients can be written as

$$C_D=C_{Dfb}+\pi a_{0x}/2, \qquad C_L=C_{Lfb}+\pi a_{0y}/2, \tag{4}$$

where subscript *fb* stands for fixed body (understood in an inertial system) [13]. In Eq. (4) a_{0x} and a_{0y} accelerations are the second time derivatives of cylinder displacements x_0, y_0 given in Eq. (1). Since a_{0x} and a_{0y} are T-periodic functions ($T=1/f$), their time-mean (TM) values vanishes, resulting in identical TM values for lift and drag in the two systems.

The non-dimensional mechanical energy transfer E originally introduced in [3] for a transversely oscillating cylinder is extended for a general 2-DoF motion of the cylinder in [11]:

$$E = \frac{2}{\rho U^2 d^2}\int_0^T \mathbf{F}\cdot\mathbf{v}_0 \mathrm{d}\,t = \int_0^T \left(C_D\, v_{0x} + C_L\, v_{0y}\right)\mathrm{d}\,t\,, \tag{5}$$

where T ($=1/f$) is the motion period, $\mathbf{F}$ is the force vector per unit length of cylinder, $\mathbf{v_0}=(v_{0x},v_{0y})$ are the velocity vector of the cylinder.

3. RESULTS

During the systematic investigations the value of amplitude ratio ε is kept constant at 0, 0.1, 0.2, 0.3, 0.4 and 0.5 at Re=150 and 200 and at frequency ratios of FR=0.8, 0.9 and 1.0 while the transverse oscillation amplitude A_y is varied. Only locked-in cases are considered. Larger ε values mean a "thicker" elliptical path but even the largest ε value investigated ensures a relatively slender elliptical path. First the effects of flow parameters on the TM values of lift (C_L) and drag (C_D) coefficients will be shown, then effects of the mechanical energy transfer E, and finally the vicinity of a jump (due to a switch in the vortex structure) will be investigated.

3.1 Effects of flow parameters on force coefficients

The time-mean (TM) and root-mean square (rms) values of lift, drag and base pressure coefficients were investigated but due to lack of space only TM of lift and drag will be shown here. Figure 3 shows the TM of lift at Re=150 and 200 for FR=0.8 for different amplitude ratios (ε) against the transverse oscillation amplitude A_y. The value $\varepsilon=0$ (eps=0 in the figure) means pure transverse oscillation. As can be seen in the figures, up to the relatively large value of A_y 0.7 for Re=150 and 0.6 for Re=200, the TM of lift is zero due to 2S shedding (two single vortices are shed in a period [1]), as was found in [14]. Around that A_y value the vortex structure changes from 2S to P+S (a pair of vortices and a single vortex shed in one period [1]) and with the breaking of the symmetry, the TM of C_L ceases to be zero. This fully harmonizes with the findings in [15]. For larger ε values the TM of C_L is not zero; it

increases with A_y, first slightly and then steeply; jumps can be seen for some ε values (ε=0.3, 0.4 and 0.5 for Re=150 and ε=0.2, 0.3 and 0.5 for Re=200). At these points a tiny change in the A_y values results in large changes in the TM of lift; this is probably a symptom of switch in the vortex structure. There are two attractors in this non-linear system, each with a basin of attraction. If the sets of parameters are near to the boundary separating the two basins of attractions, then a tiny change in a single parameter might be sufficient to change the attractor [16]. At Re=200 the upper synchronization limits for ε=0.4 and 0.5 are around A_y=0.6, hence the curves terminate here. There is not a very clear tendency for the effect of ε on TM of lift; at Re=150 the TM of C_L mainly increases with ε but for Re=200 this is true just for A_y values larger than 0.6.

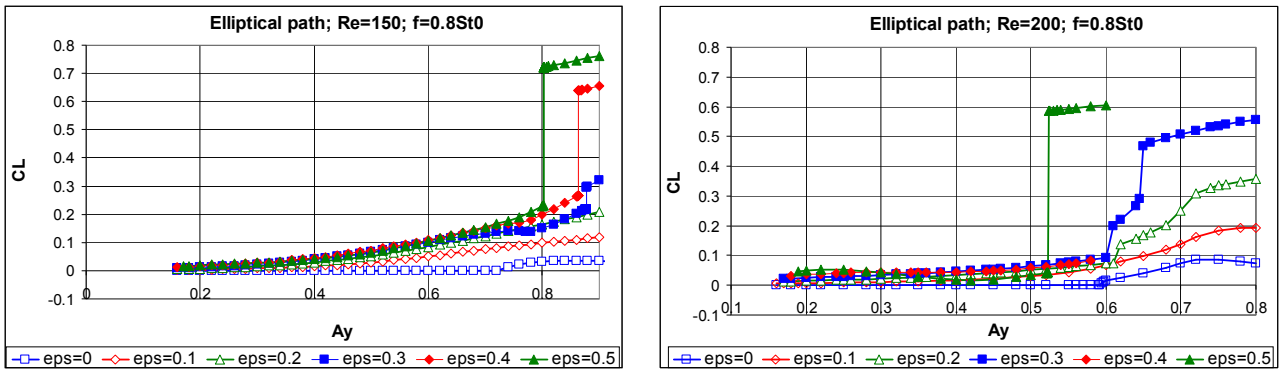

Figure 3: (a) Time-mean of lift for (a) Re=150 and (b) Re=200 against A_y at FR=0.8

Figure 4 shows the curves for FR=0.9, which in general display similar tendencies to those seen in FR=0.8. However, for Re=150: the effect of ε is more pronounced and TM of lift increases with ε; the upper lock-in boundary reduces for ε=0.4 and 0.5. For Re=200 the location of the jump for the largest ε value of 0.5 moves to lower A_y values (between 0.3 and 0.4). The lower lock-in boundary moves to smaller A_y values compared to FR=0.8, as was also found in [15] for transverse cylinder oscillation.

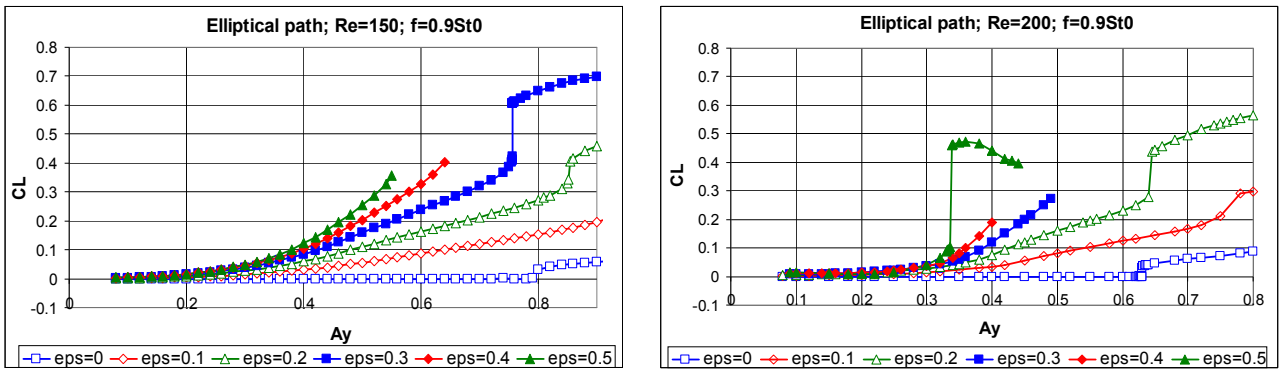

Figure 4: (a) Time-mean of lift for (a) Re=150 and (b) Re=200 against A_y at FR =0.9

Figure 5 shows curves for FR=1. In the case of Re=150 the curves belonging to different ε values spread more than for smaller frequency ratios and for the largest three ε values the upper limits for lock-in are shifted to even smaller A_y values. For Re=200 flow is locked-in over the investigated A_y domain only at ε=0 and 0.1; for ε=0.2-0.5 there is no lock-in over a large part of the computational domain.

Results for the TM of drag are shown for only two frequency ratios, FR=0.8 and 1.0 (see Figs. 6 and 7). Figure 6(a) for Re=150 and FR=0.8 shows that the shape of the cylinder path (ε) does not have much effect on the TM of drag; the curves almost coincide with each other, especially below the small jumps at the A_y values seen in Fig. 3(a) too. For the Re=200 case the effect of ε is more pronounced and the TM of C_D seems to increase with ε and A_y (not considering the jumps, which are at the same A_y values as in Fig. 3(b)). Figure 7(a) shows the TM of drag for Re=150 and FR=1.0. The shape of the curve is similar to the FR=0.8 equivalent shown in Fig. 6(a) but the curve shifts to higher drag values.

Jumps occur at the same A_y values as in Fig. 5(a). Figure 7(b) shows the TM of drag for FR=1.0. Just as in Fig. 5(b), the flow is locked-in over the investigated A_y domain only at ε=0 and 0.1 for Re=200. Some isolated lock-in points/short curves appear at this Re and FR (see also Fig. 5(b)).

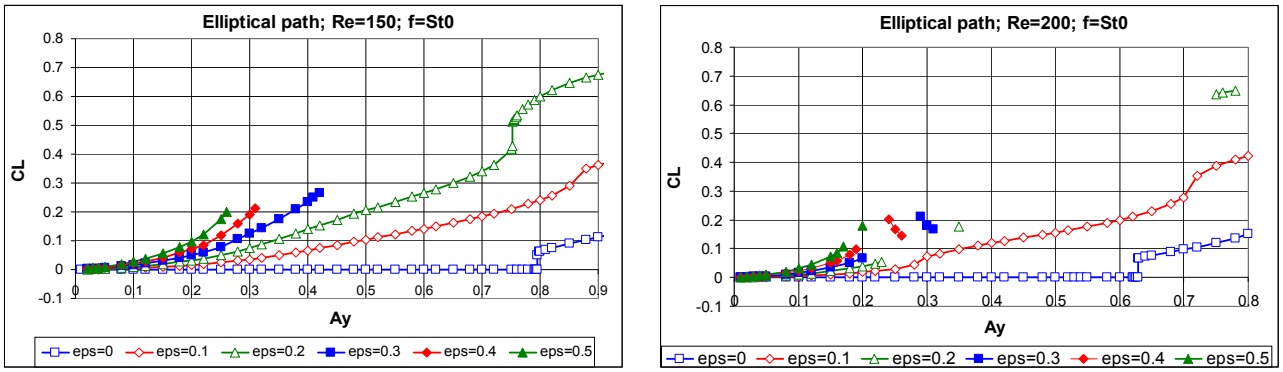

Figure 5: (a) Time-mean of lift for (a) Re=150 and (b) Re=200 against A_y at FR =1.0

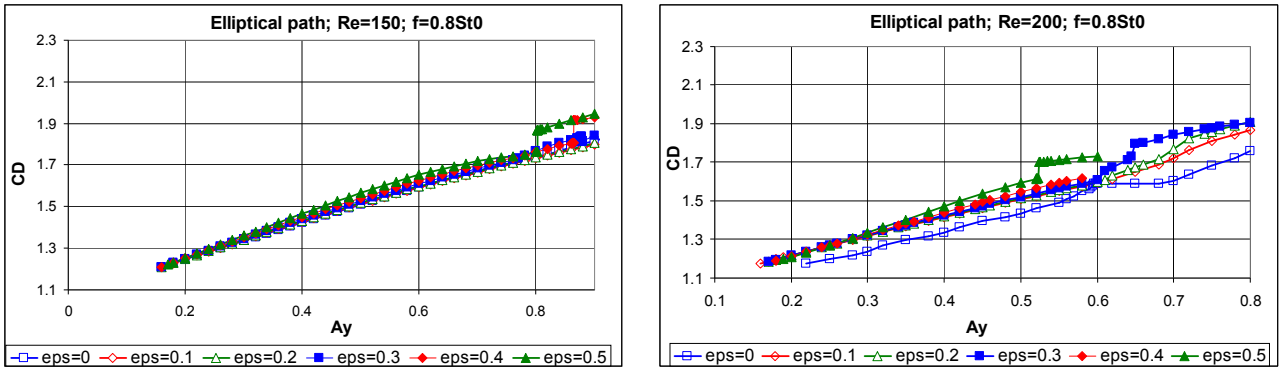

Figure 6: (a) Time-mean of drag for (a) Re=150 and (b) Re=200 against A_y at FR =0.8

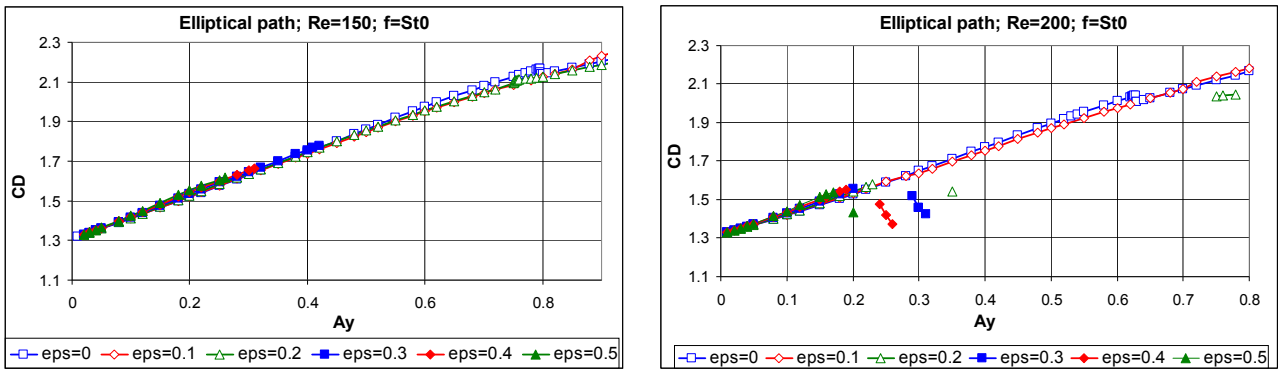

Figure 7: (a) Time-mean of drag for (a) Re=150 and (b) Re=200 against A_y at FR =1.0

3.2 Mechanical energy transfer between fluid and cylinder

Let us see now how the mechanical energy transfer E, defined by Eq. (5), depends on the parameters of flow: frequency ratio FR=f/St$_0$, amplitude ratio ε=A$_x$/A_y; Re, and transverse cylinder oscillation amplitude A_y.

3.2.1 Effects of frequency and amplitude ratios for Re=150

The mechanical energy transfer E against A_y was investigated for FR=0.8, 0.9 and 1.0 and for the six amplitude ratio values. Figure 8 shows the case of FR=0.8. As can be seen in Fig. 8(a), E is negative for the largest part of the parameter domain and its absolute value increases with ε and A_y, meaning that the larger the amplitude and "thicker" the cylinder paths the larger the energy extracted from the cylinder. Small positive values can be seen only for amplitudes below 0.45 (see also Fig 8(b)). Jumps

in E occur just for ε=0.4 and 0.5 (see also Fig 3(a)). Figure 8(b) shows the part of Fig. 8(a) in which E is positive. Only curves belonging to the four smaller ε have positive E values. For each curve E has a maximum and E decreases with increasing ε values. As was mentioned earlier, such positive energy transfer may be a potential source of vortex-induced vibration (VIV) for a freely vibrating system [4].

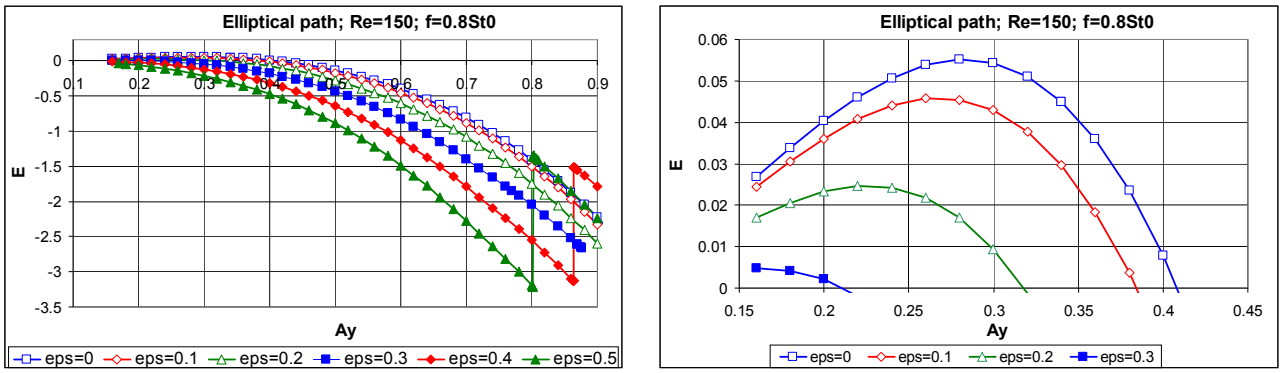

Figure 8: Mechanical energy transfer E against A_y at FR=0.8, Re=150 (a); zoom in on positive E (b)

Figure 9 shows the case of FR=0.9. The tendencies are very similar to those in Fig. 8, although the curves group together more at FR=0.9 than at FR=0.8. The locations of jumps are identical to those in Fig. 4(a). When we zoom-in on positive E values (see Fig 9(a)) we can see that all curves have positive E and E is almost three times larger than for FR=0.8. Again, as the cylinder path thickens (see ε) the E peaks decrease. The largest E peak is for transverse cylinder oscillation (ε=0).

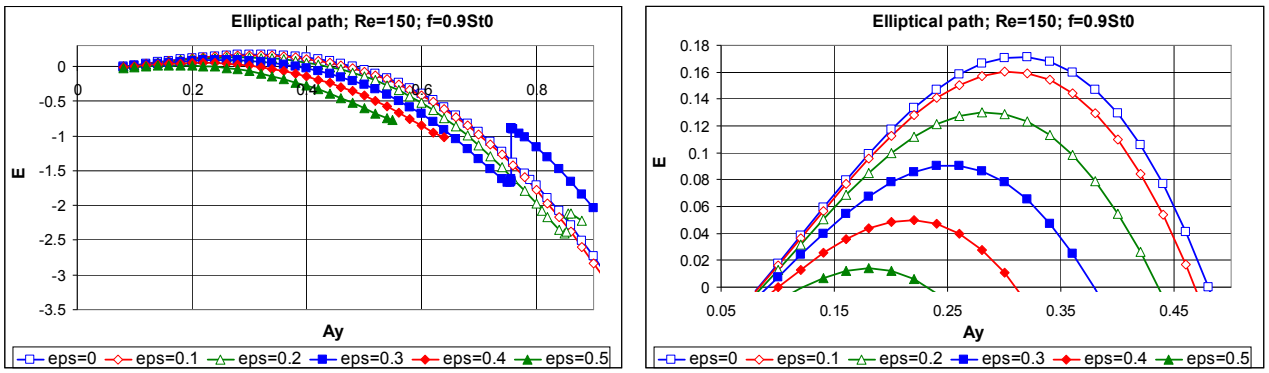

Figure 9: Mechanical energy transfer E against A_y at FR=0.9, Re=150 (a); zoom in on positive E (b)

Finally, Fig. 10 shows the case of FR=1. Like in Fig. 5(a), for the three largest ε values the upper lock-in boundaries are between A_y=0.25 and 0.42. The curves group together, even for the zoomed in curves (Fig. 10(b)), unlike for smaller FR cases. It can thus be seen that the path shape (ε) does not have much effect on E and that the peak value of E is much higher in this case than for smaller frequency ratios. The $0< A_y<0.53$ domain can lead to VIV for the equivalent free vibration cases.

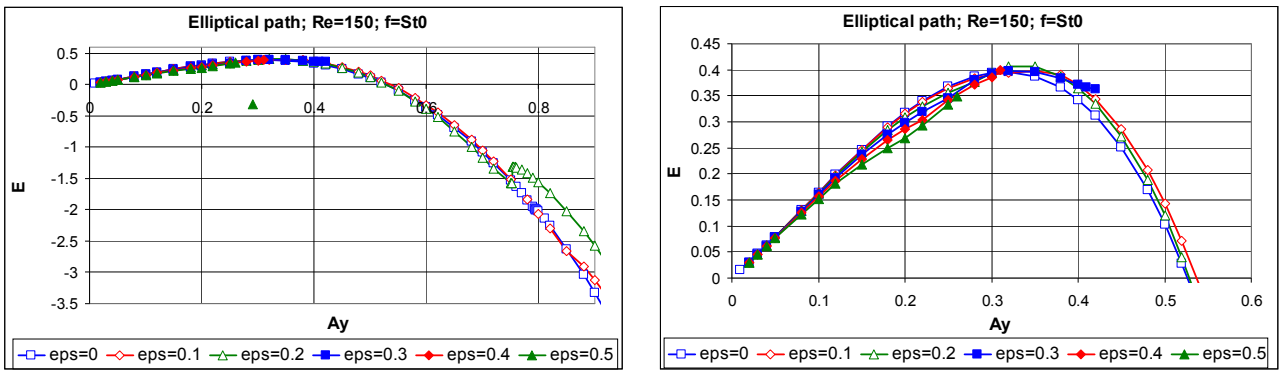

Figure 10: Mechanical energy transfer E against A_y at FR=1.0, Re=150 (a); zoom in on positive E (b)

3.2.2 Effects of frequency and amplitude ratios for Re=200

Results are shown here for Re=200. Figures 11, 12 and 13 show the cases of FR=0.8, 0.9 and 1.0, respectively. A general remark is that curves become more irregular at Re=200 than at Re=150. In Fig. 11(a) (similarly to Fig. 3(b)) the effect of ε is pronounced; curves belonging to different ε values can be distinguished from each other easily. ε=0.4 had only negative values, and thus does not appear in the zoom in version of the figure for positive values (Fig. 11(b)). The left side of the figure shows a similar tendency to its Re=150 counterpart (see Fig. 8(b)), but a jump also appears for ε=0.5 in Fig. 11(b).

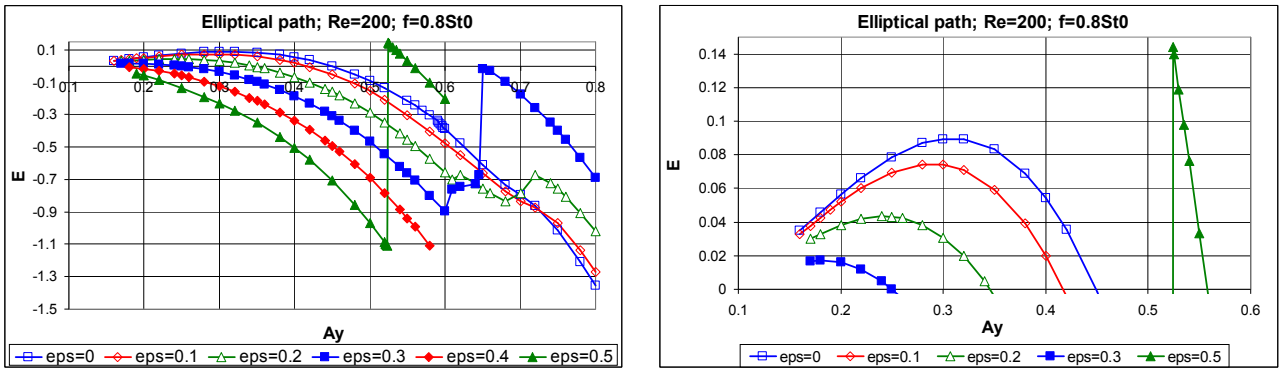

Figure 11: Mechanical energy transfer E against A_y at FR=0.8, Re=200 (a); zoom in on positive E (b)

The FR=0.9 case can be seen in Fig. 12. The larger part of the domain is again characterized by negative E values (see Fig. 12(a)) and part of the curves terminate at intermediate A_y values due to the upper lock-in limit. Not considering the jump in the ε=0.5 curve, the tendency is similar to earlier: the peak in E decreases with ε; the tallest peak is twice as high as for FR=0.8. FR=1 results are shown in Fig. 13; above A_y=0.2 the flow is locked in only for ε=0 and 0.1. Fig. 13(b) shows that the shape of the path (ε) does not influence E: the different ε curves collapse to a single curve up to about A_y=0.2. Here the ε=0.1 curve has the highest E peak, at about 0.6, which is about three times larger than for FR=0.9.

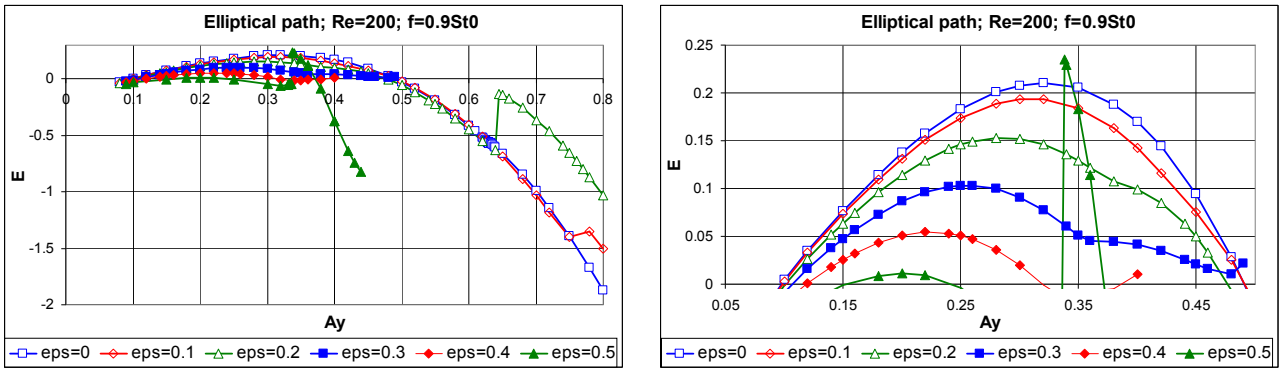

Figure 12: Mechanical energy transfer E against A_y at FR=0.9, Re=200 (a); zoom in on positive E (b)

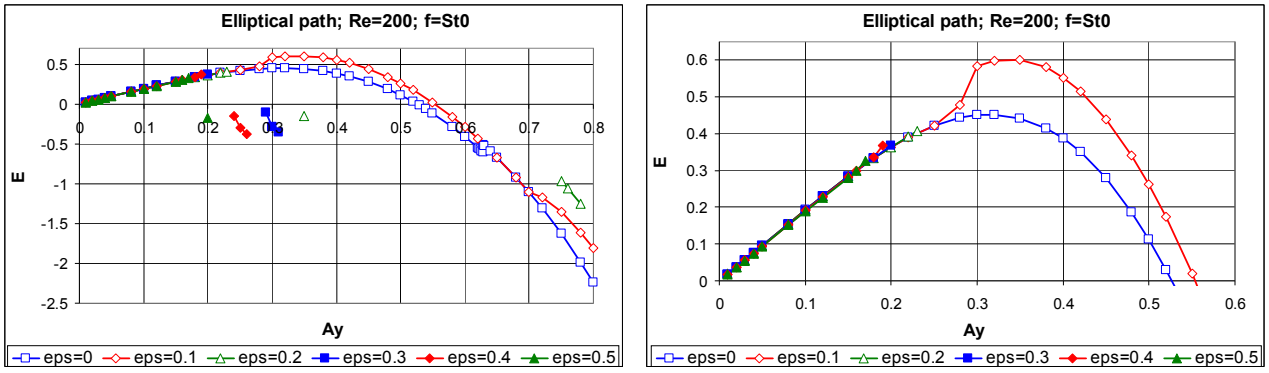

Figure 13: Mechanical energy transfer E against A_y at FR=1.0, Re=200 (a); zoom in on positive E (b)

3.2.3 Frequency ratio and Reynolds number effects

In this subsection the positive mechanical energy transfer E is shown against A_y for the three FR values investigated at ε=0.2 for both Reynolds numbers. Fig. 14(a) shows results for Re=150 and Fig. 14(b) Re=200. The two sets of curves are not very different from each other, except that for Re=200 the FR=1 case is not fully locked-in. As can be seen in the figures, these positive E values are limited to moderate A_y values, and, as we have seen earlier, peak E values increase with FR.

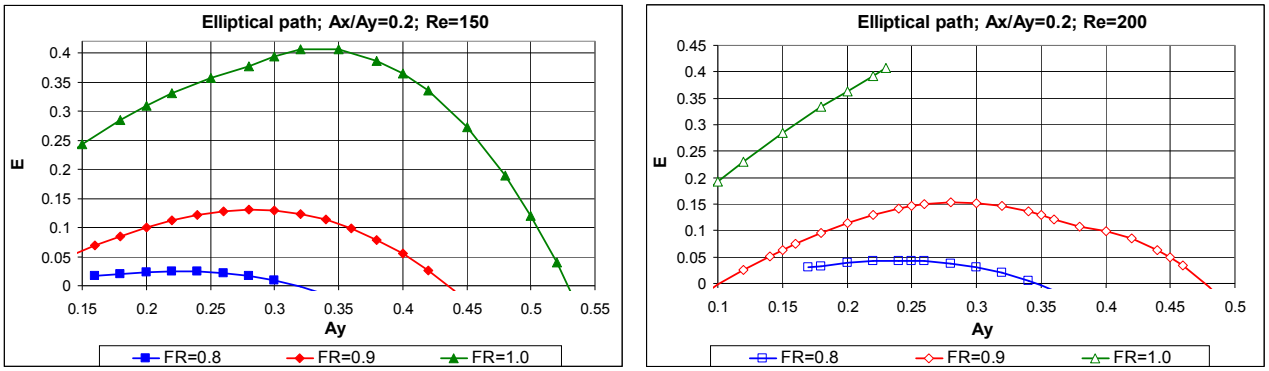

Figure 14: Mechanical energy transfer against A_y at ε =0.2, FR=0.8, 0.9, 1.0, Re=150 (a) and 200 (b)

Although only two Reynolds numbers were investigated, we can still see some Reynolds number effects in Fig. 15. Since all FR values showed similar results, just FR=0.9 is shown. Figure 15(a) shows positive E values against A_y for Re=150 and 200 at ε=0.2 and Fig. 15(b) the same for transverse oscillation (ε=0). As can be seen the Re= 200 curves are mainly above Re=150 curves, indicating that the increase in Re increases the positive E peak. On the other hand for the transversely oscillating cylinder the E peaks are higher for both Re than those for a slender elliptical path (ε=0.2).

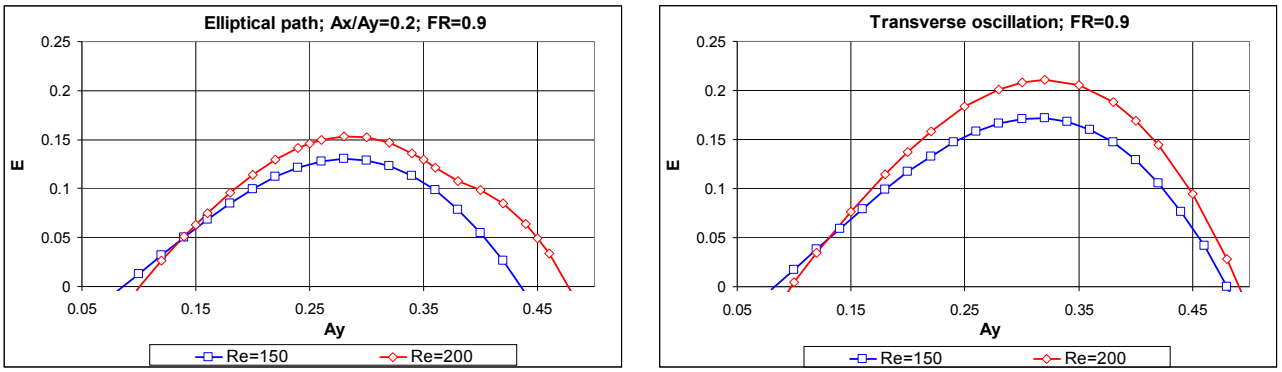

Figure 15: Mechanical energy transfer E against A_y at FR=0.9, Re=150 and 200, ε=0.2 (a) and 0 (b)

3.3 Pre- and post-jump analysis

The vicinity of a jump were investigated by different means, but only two will be shown here: (drag,lift) limit cycle curves and vorticity contours for pre- (A_{y-}) and post-jump (A_{y+}) amplitude values. The data for the jump shown here are Re=200; FR=0.9; ε=0.5; A_{y-}=0.336; A_{y+}=0.338; the jump can be seen clearly in Fig. 4(b). When two time-dependent functions become periodic their limit cycle curves can be determined by eliminating the time from them. In Fig. 16 the (C_{Dfb},C_{Lfb}) limit cycle curves for A_{y-} (thick line) and A_{y+} (thin line) are given. A tiny change in the A_y value leads to a very substantial change in the curves, since the boundary between the two basins of attractions is crossed when A_y is changed from A_{y-} to A_{y+} [16].

Vorticity contours are shown in Fig. 17 for the A_{y-} (left) and A_{y+} (right) amplitude values. The grey lines indicate negative vorticity values (rotating clockwise), and the black are positive (anticlockwise). The contours are taken at the same instant (t=1800≈316.5 T) and thus at the same cylinder positions. The substantial difference is obvious, suggesting a switch in the vortex structure.

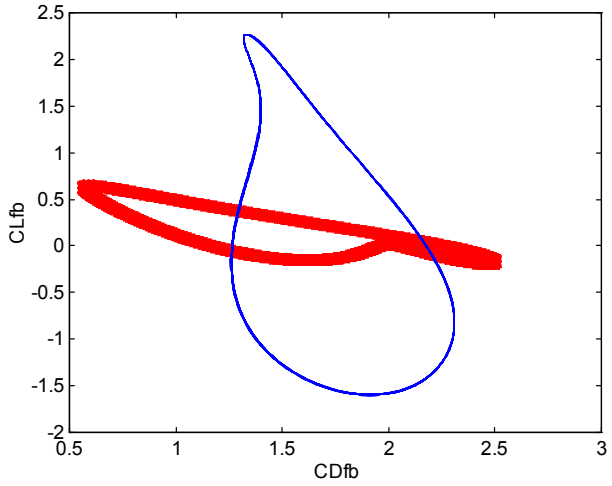

Figure 16: The (C_{Dfb},C_{Lfb}) limit cycle curves for pre-jump (thick line) and post-jump (thin line) A_y values (Re=200; FR=0.9; ε=0,5; A_{y-}=0.336; A_{y+}=0.338)

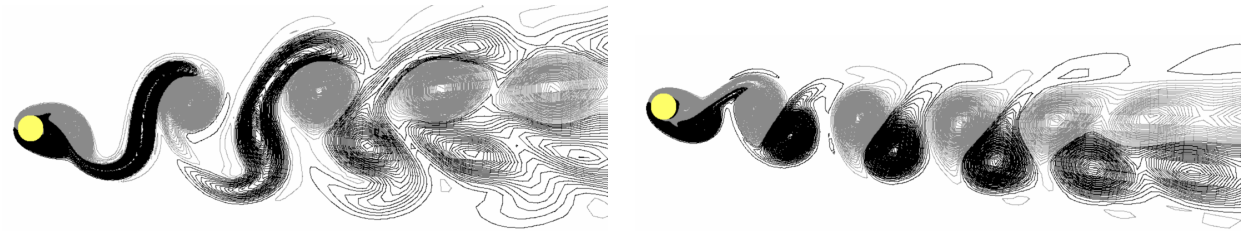

Figure 17: Vorticity contours: left pre-jump (A_{y-} =0.336); right post-jump (A_{y+} =0.338)

4. CONCLUSIONS

Flow around a circular cylinder forced to follow a slender elliptical path is investigated numerically at frequency ratios FR=0.8, 0.9 and 1, Re=150 and 200, and amplitude ratios $\varepsilon=A_x/A_y$=0, 0.1, 0.2, 0.3, 0.4 and 0.5 in the lock-in domain. Mechanical energy transfer E and time history of lift and drag are plotted against transverse oscillation amplitude A_y while other parameters are kept constant.

From the results it can be stated that:

- jumps occur just at relatively large A_y values;
- drag is not much influenced by the shape of the cylinder path (ε);
- E is negative in the largest part of the parameter domain; and
- positive E values are confined to moderate A_y values ($A_y < 0.5$).

The height of the E peak is influenced by several parameters:

- the E peak increases with FR;
- the E peak increases with Re;
- the E peak decreases with ε;
- at FR=0.8 ε has largest effect on the E peak, less at FR=0.9, and almost no effect at FR=1 (where curves group together).

In addition, it was observed that:

- curves become more irregular for Re=200;
- jumps in the curves indicate a switch in the vortex structure, as supported by limit cycle curves and vorticity contours.

Future investigations could include computations at further Re numbers, although increasing Reynolds number values may be problematic due to three-dimensional instabilities, which seem to have begun to appear even at Re=200. The frequency ratio domain could be extended as well.

ACKNOWLEDGEMENTS

The support provided by the Hungarian Scientific Research Fund for project OTKA K 76085 is gratefully acknowledged. The author would like to thank Mr. L. Daróczy for designing the flow visualization software used in Fig. 17. The work was carried out as part of the TÁMOP-4.2.1.B-10/2/KONV-2010-0001 project in the framework of the New Hungarian Development Plan. The realization of this project is supported by the European Union, co-financed by the European Social Fund.

REFERENCES

[1] C.H.K. Williamson and A. Roshko, Vortex formation in the wake of an oscillating cylinder, *Journal of Fluids and Structures*, **2**, pp. 355-381, 1988.

[2] X.Y. Lu and C. Dalton, Calculation of the timing of vortex formation from an oscillating cylinder, *Journal of Fluids and Structures*, **10**, pp. 527-541, 1996.

[3] H.M. Blackburn and R.D. Henderson, A study of two-dimensional flow past an oscillating cylinder, *Journal of Fluid Mechanics*, **385**, pp. 255-286, 1999.

[4] J.S. Leontini, B.E. Stewart, M.C. Thompson and K. Hourigan, Predicting vortex-induced vibration from driven oscillation results, *Applied Mathematical Modelling,* **30**, pp. 1096-1102, 2006.

[5] A. Okajima, A. Nakamura, T. Kosugi, H. Uchida and R. Tamaki, Flow-induced in-line oscillation of a circular cylinder, *European Journal of Mechanics B/Fluids*, **23**, pp. 115-125, 2004.

[6] Q.M. Al-Mdallal, K.P. Lawrence and S. Kocabiyik, Forced streamwise oscillations of a circular cylinder: Locked-on modes and resulting fluid forces, *Journal of Fluids and Structures*, **23**, pp. 681-701, 2007.

[7] N. Jauvtis and C.H.K. Williamson, The effect of two degrees of freedom on vortex-induced vibration and at low mass and damping, *Journal of Fluid Mechanics*, **509**, pp. 23-62, 2004.

[8] A. Sanchis, G. Sælevik and J. Grue, Two-degree-of-freedom vortex-induced vibrations of a spring-mounted rigid cylinder with low mass ratio, *Journal of Fluids and Structures*, **24**, pp. 907-919, 2008.

[9] S. Kheirkhah, S. Yarusevych and S. Narasimhan, Orbiting response in vortex-induced vibrations of a two-degree-of-freedom pivoted circular cylinder, *Journal of Fluids and Structures*, **28**, pp. 343–358, 2012.

[10] E. Didier and A.R.J. Borges, Numerical predictions of low Reynolds number flow over an oscillating circular cylinder, *Journal of Computational and Applied Mechanics*, **8**(1), pp. 39-55, 2007.

[11] L. Baranyi, Numerical simulation of flow around an orbiting cylinder at different ellipticity values, *Journal of Fluids and Structures*, **24**, pp. 883-906, 2008.

[12] R.D. Blevins, *Flow-Induced Vibrations*, 2nd Ed., Krieger Publishing Company, 1990.

[13] L. Baranyi, Lift and drag evaluation in translating and rotating non-inertial systems, *Journal of Fluids and Structures*, **20**, pp. 25-34, 2005.

[14] L. Baranyi, Sudden and gradual alteration of amplitude during the computation for flow around a cylinder oscillating in transverse or in-line direction, *Proc. ASME 2009 Pressure Vessels and Piping Conference, Symposium on Flow-Induced Vibration*, on CD ROM, Prague, pp.1-10, Paper No. PVP2009-77463, 2009.

[15] J.S. Leontini, B.E. Stewart, M.C. Thompson and K. Hourigan, Wake state and energy transitions of an oscillating cylinder at low Reynolds number, *Physics of Fluids*, **18**, 067101, 2006.

[16] S.H. Strogatz, *Nonlinear Dynamics and Chaos*, Westview Press, 1994.